INORGANIC CHEMISTRY FRONTIERS

RESEARCH ARTICLE

View Article Online
View Journal | View Issue

Cite this: *Inorg. Chem. Front.*, 2024, **11**, 3245

New ultraviolet transparent rare-earth borates with enhanced birefringence induced by cation chemical substitution†

Guanglian Sun, Xiaofang Qi,* Hongping Wu,* Zhanggui Hu, Jiyang Wang and Yicheng Wu

Received 2nd April 2024,
Accepted 14th April 2024

DOI: 10.1039/d4qi00840e

rsc.li/frontiers-inorganic

Birefringence determined by optical anisotropy is one of the most pivotal and fundamental performance of optical materials. However, optimizing the birefringence remains a significant challenge. Herein, a simple and effective method of cation chemical substitution for improving the birefringence has been accomplished and three Y-based borates, namely, $LiNa_2Y(BO_3)_2$, $RbNa_2Y(BO_3)_2$ and $RbSrY(BO_3)_2$, were successfully synthesized. They all have deep-ultraviolet (DUV) cutoff edges below 190 nm. Single-crystal analysis reveals that $LiNa_2Y(BO_3)_2$ and $RbNa_2Y(BO_3)_2$ possess three-dimensional (3D) frameworks with small channels filled by alkali metal cations, whereas $RbSrY(BO_3)_2$ features a two-dimensional (2D) layered structure separated by alkali metal and alkali-earth metal cations. The birefringence exhibits a progressive doubling increase from $LiNa_2Y(BO_3)_2$ (0.017@532 nm) to $RbNa_2Y(BO_3)_2$ (0.033@532 nm) and then to $RbSrY(BO_3)_2$ (0.070@532 nm). Using cation size arguments, coordination environment, and the arrangement of groups demonstrate that cation substitution have a decisive effect on the birefringence enhancement. In addition, other optical and thermal properties of the three title compounds were characterized. The structure–property relationships were analyzed by the first-principles calculations.

Introduction

Birefringence refers to the phenomenon that a beam of natural light passing through an anisotropic crystal is split into two beams of polarized light with different refractive indices.[1–4] As the key optical property of photoelectric functional materials, birefringence plays an indispensable role in the field of both linear and nonlinear optics (NLO).[5–10] In the realm of traditional linear optics, birefringence, due to its capability of modulating polarized light, has become extensively integrated in various polarization devices such as electro-optic modulators, electro-optic switches and optical isolators.[11–13] Additionally, for the laser-dominated NLO field, an appropriate birefringence, such as $\Delta n > 0.03$ for the infrared NLO materials, 0.06–0.1 for ultraviolet (UV) or deep ultraviolet (DUV) ones, can offset the phase mismatch caused by dispersion, achieving phase matching (PM) of NLO crystals.[14] After decades of continuous development, many materials with enhanced birefringence have been widely used in the near-infrared (NIR) and visible regions, such as YVO_4,[15] TiO_2,[16] $LiNbO_3$,[17] and $CaCO_3$.[18] However, in UV and DUV regions, the material possessing large birefringence is still quite scarce.[19–22] Although MgF_2 [23] as a birefringent material possessing DUV transparent window (~110 nm) has been commercialized, the insufficient birefringence (Δn = 0.012@532 nm) remains an obstacle to its widespread application.[24,25] Therefore, optimizing the birefringence of UV/DUV materials is still a prominent focus in contemporary materials research.

From the perspective of structure–performance relationships, birefringence mainly originates from the anisotropy of structural polarization.[26,27] Generally, introducing strongly distorted basic building units (BBUs) into the structure is conducive to increase the birefringence of materials.[28–30] These BBUs typically consist of the polyhedra with cations susceptible to second-order Jahn–taller (SOJT) effects, including d^0 transition metals (Nb^{5+}, Mo^{6+}, W^{6+}, *etc.*) and stereochemically active lone pair (SCALP) cations (Pb^{2+}, Sn^{2+}, Sb^{3+}, *etc.*).[31–34] The strategy has proven effective by reported oxides with large birefringence, such as the $K_3Nb_3Ge_2O_{13}$ (0.196@546 nm),[35] $Sn_2B_5O_9Cl$ (0.196@546 nm),[36] and $Hg_4(Te_2O_5)(SO_4)$ (0.542@546 nm).[37] However, an unwanted red shift of the cutoff edge is always caused by these cations.[38–40] As a result, the strategy is not suitable to enhance the birefringence of UV, especially DUV optical materials. Relatively, the π-conjugated

Tianjin Key Laboratory of Functional Crystal Materials, Institute of Functional Crystal, Tianjin University of Technology, Tianjin 300384, China.
E-mail: wuhp2022@163.com

† Electronic supplementary information (ESI) available. CCDC 2327205–2327207 for $LiNa_2Y(BO_3)_2$, $RbNa_2Y(BO_3)_2$ and $RbSrY(BO_3)_2$. For ESI and crystallographic data in CIF or other electronic format see DOI: https://doi.org/10.1039/d4qi00840e

planar $[BO_3]^{3-}$ and $[B_3O_6]^{3-}$ anionic groups, possessing large anisotropy and wide transparency window, make great contributions to the enhanced birefringence and short UV cutoff edge.[41–44] Recently, some research has also proven that the rare-earth cations with closed-shell electronic configurations such as Y^{3+} and Sc^{3+} play a positive role in achieving both improved birefringence and wide UV transparent windows.[45,46]

In this study, to achieve the effect of killing two birds with one arrow, rare-earth borate was considered by our research group. Meanwhile, alkali metal and alkali-earth metal cations without d–d electron transition were introduced in rare-earth borates on the one hand for widening the UV transparent window and on the other hand for adjusting the polymerization of anion groups. Three new alkali/alkali-earth Y-based borates with isolated BO_3 triangles, namely, $LiNa_2Y(BO_3)_2$, $RbNa_2Y(BO_3)_2$ and $RbSrY(BO_3)_2$, have been successfully synthesized by combining cation number effect with the cation chemical substitution. Three compounds exhibit similar stoichiometry, but they crystallize in different space groups ($LiNa_2Y(BO_3)_2$ & $P2_1/n$; $RbNa_2Y(BO_3)_2$ & $Pnma$; $RbSrY(BO_3)_2$ & $P2_1/m$). Birefringence calculations show that their birefringence values exhibit doubling of increase from 0.017@532 nm of $LiNa_2Y(BO_3)_2$ to 0.033@532 nm of $RbNa_2Y(BO_3)_2$, and then to 0.070@532 nm of $RbSrY(BO_3)_2$. The substitution of alkali metal/alkali-earth metal cations cause the different arrangement of B–O and Y–O groups that has a great influence on the birefringence of the materials, which is rarely reported in rare-earth borates. Therefore, in this report, we will discuss the effect of cation substitution on the structure and then on the birefringence in detail. In addition, the structures, properties, and the first-principles calculations for these materials are reported. This work will provide some new insights for the designing of UV or DUV optical materials with large birefringence.

Results and discussion

The structures of three compounds are shown in Fig. 1. $LiNa_2Y(BO_3)_2$ crystallizes in the monoclinic space group $P2_1/c$ (Table S1†). Its asymmetric unit contains one crystallographic-independent Li, two Na, one Y, two B, and six O atom(s). All the B atoms are connected to three O atoms to form isolated BO_3 triangles with the B–O distances ranging from 1.353(8) to 1.396(7) Å. The Y atoms are linked to eight O atoms to build the irregular YO_8 polyhedra with Y–O distances of 2.270(5)–2.517(4) Å. Further, the YO_8 polyhedra are interconnected by the sharing of oxygen atoms to form $^1_\infty[YO_6]$ layers, which are linked with BO_3 triangles to construct a final three-dimensional (3D) framework with channels filled by Li^+ and Na^+ cations to balance charges (Fig. 1a). The Li atoms are connected to five oxygen atoms and the Li–O distances range from 1.938(14) to 2.313(13) Å. The Na(1) and Na(2) atoms are in sevenfold and fivefold coordination environments, respectively, with distances in the range of 2.196(5)–2.948(5) Å. According to Brown's formula,[47] the bond valence sum (BVS) analyses for every atom result in values of 0.96 for Li^+, 1.02–1.06 for Na^+, 3.09 for Y^{3+}, 2.94–2.98 for B^{3+}, and 1.82–2.05 for O^{2-} (Table S2†). These are all consistent with the expected oxidation states.

$RbNa_2Y(BO_3)_2$ crystallizes in the orthorhombic space group $Pnma$, and its asymmetric unit has one crystallographically independent Rb, one Na, one Y, two B, and five O atom(s). Y

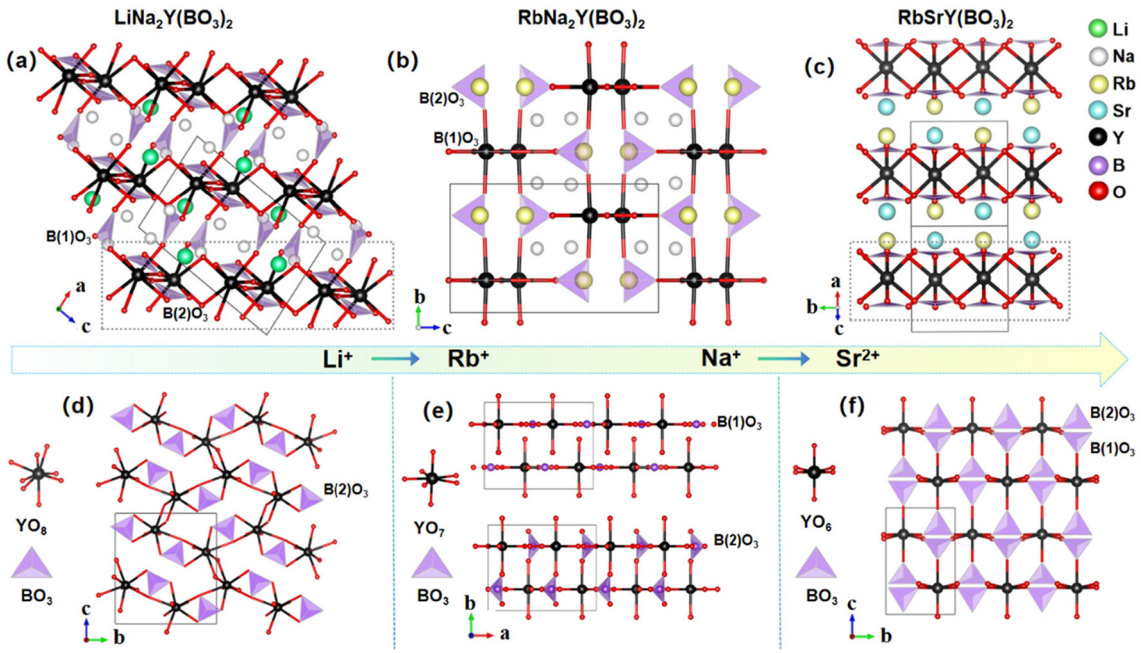

Fig. 1 Structures of (a) $LiNa_2Y(BO_3)_2$, (b) $RbNa_2Y(BO_3)_2$ and (c) $RbSrY(BO_3)_2$. Connected modes of Y–O and B–O groups in (d) $LiNa_2Y(BO_3)_2$, (e) $RbNa_2Y(BO_3)_2$ and (f) $RbSrY(BO_3)_2$.

atoms are coordinated with seven O atoms to construct YO_7 polyhedra, which are linked together to build $^1_\infty[YO_6]$ infinite chains. The neighboring $^1_\infty[YO_6]$ chains are connected by isolated BO_3 triangles to construct a 3D framework with tunnels located by Rb and Na cations (Fig. 1b). The Rb and Na atoms are in seven-coordinated environments to form the AO_7 (A = Rb, Na) polyhedra. The B–O, Y–O, Rb–O and Na–O distances range from 1.361(14) to 1.415(13) Å, 2.232(4) to 2.360(7) Å, 2.762(7) to 3.631(2) Å, and 2.461(6) to 3.019(6) Å, respectively (Table S3†). Bond valence calculations resulted in values of 1.11, 0.79, 3.28, 2.89–2.98, and 1.91–2.01 for Rb^+, Na^+, Y^{3+}, B^{3+}, and O^{2-}, respectively (Table S2†).

$RbSrY(BO_3)_2$ crystallizes in the monoclinic space group $P2_1/m$. In the asymmetric unit, there is one unique Rb, one unique Sr, one unique Y, two unique B and four unique O atom(s). The isolated YO_6 octahedra and BO_3 construct a two-dimensional (2D) layered structure separated by Rb^+ and Na^+ cations (Fig. 1c). Both Rb and Sr atoms are coordinated with nine oxygen atoms. The bond distances are as follows: B–O: 1.361(14) to 1.415(13) Å, Y–O: 2.228(9) to 2.267(9) Å, Rb–O: 2.859(3) to 3.153(7) Å, Sr–O: 2.709(6) to 2.793(6) Å (Table S3†). The BVS analyses for each atom in $RbSrY(BO_3)_2$ result in values of 1.09 for Rb^+, 1.75 for Sr^{2+}, 3.26 for Y^{3+}, 3.01 for B^{3+}, and 2.01–2.14 for O^{2-} (Table S2†). Clearly, the BVSs of Y^{3+} in $RbNa_2Y(BO_3)_2$ and $RbSrY(BO_3)_2$ are 3.28 and 3.26, respectively, which are slightly higher than their expected values. In fact, the large BVSs for Y^{3+} can also be found in other compounds, such as 3.32 in $Na_3Y_3(BO_3)_4$, 3.22 in $KBaY(BO_3)_2$, 3.20 in $K_3YB_6O_{12}$ and 3.21 in $K_7CaY_2(B_5O_{10})_3$. Thus, the BVSs for Y^{3+} are within a reasonable range.

Influence of the cation size on the framework structures

Although the three compounds have similar formula, they crystallize in different space groups, *i.e.*, $LiNa_2Y(BO_3)_2$ & $P2_1/n$, $RbNa_2Y(BO_3)_2$ & *Pnma*, $RbSrY(BO_3)_2$ & $P2_1/m$ due to cation substitution. All the title compounds contain isolated BO_3 triangles and Y–O polyhedra. The structural differences will be discussed in detail in the following two aspects: **(i) Different arrangements and connected modes of B–O and Y–O groups.** All three structures contain two crystallographically independent BO_3 units, namely, $B(1)O_3$ and $B(2)O_3$. In $LiNa_2Y(BO_3)_2$, $B(1)O_3$ are connected with Y–O layers to form a 3D network, while $B(2)O_3$ triangles are localized in the interlayers and feature a reversed arrangement (Fig. 1d). In $RbNa_2Y(BO_3)_2$, the $B(2)O_3$ triangles are responsible for linking Y–O chains to form a 3D framework, while $B(1)O_3$ groups are embedded between two YO_7 polyhedra in the Y–O chain (Fig. 1e). In $RbSrY(BO_3)_2$, $B(1)O_3$ and $B(2)O_3$ triangles adopt a coplanar configuration with an oppositely aligned arrangement to connect with isolated YO_6 polyhedra, forming a 2D layered structure (Fig. 1f). In addition, the Y atoms also exhibit different coordination environments in these three structures, *i.e.*, YO_8 in $LiNa_2Y(BO_3)_2$, YO_7 in $RbNa_2Y(BO_3)_2$ and YO_6 in $RbSrY(BO_3)_2$. From $LiNa_2Y(BO_3)_2$ to $RbNa_2Y(BO_3)_2$, taken from Shannon,[48] the ionic radius of Rb^+ cation (1.56 Å) is significantly larger than that of Li^+ cation (0.59 Å). Also, the coordination number of RbO_7 polyhedra in $RbNa_2Y(BO_3)_2$ is more than that of LiO_5 in $LiNa_2Y(BO_3)_2$. Thus, the relatively low coordination of YO_7 has been observed in $RbNa_2Y(BO_3)_2$. From $RbNa_2Y(BO_3)_2$ to $RbSrY(BO_3)_2$, the radius of 9-coordinated Sr^{2+} (1.31 Å) is larger than that of 7-coordinated Na^+ (1.12 Å). Accordingly, the coordination number of Rb cation also increases from RbO_7 in $RbNa_2Y(BO_3)_2$ to RbO_9 in $RbSrY(BO_3)_2$. As such, in $RbSrY(BO_3)_2$, the coordination number of Y–O is only six-coordinated. **(ii) Cation coordination environment and linkage modes.** As shown in Fig. S1,† the alkali metal or alkaline earth-metal cations are occupied in the respective cavities formed by the Y–O six membered rings in $LiNa_2Y(BO_3)_2$ and $RbNa_2Y(BO_3)_2$ or Y–O interlayer spaces in $RbSrY(BO_3)_2$. Besides, in $LiNa_2Y(BO_3)_2$, $Na(2)O_5$ and $Na(1)O_7$ polyhedra are connected into a 3D network, and the isolated LiO_5 are located between the Na–O polyhedra, forming the final cation framework. On the other hand, in $RbNa_2Y(BO_3)_2$ and $RbSrY(BO_3)_2$, the Na-, Rb- and Sr-centered polyhedra all connected with each other to form 1D chains. These chains are further connected to form a 3D cation network in $RbNa_2Y(BO_3)_2$ and 2D layers in $RbSrY(BO_3)_2$ (Fig. S2†). To sum up, the reason for the structural changes may be induced by the cation size effect that the substituted cations with a larger cation size and higher coordination number influence the nature of the Y–O groups bonding mode to BO_3 triangles.

The UV-vis-NIR diffuse reflectance spectra are shown in Fig. 2a–c. They all have DUV transparency down to 190 nm, and the experimental bandgaps are 5.68, 5.65, and 5.56 eV, respectively. These values are comparable to those of other reported rare-earth borates, such as $K_3YB_6O_{12}$ (195 nm),[49] $Ca_4YO(BO_3)_3$ (200 nm),[50] and $K_7MY_2(B_5O_{10})_3$ (M = Ca, Sr, and Ba) (<190 nm),[51] indicating that the title compounds have potential applications in the DUV region. In addition, to reveal the different coordination environments of boron atoms, the IR spectra were measured and are depicted in Fig. 2d–f. The absorption peaks at 1351 and 1175 cm^{-1} in $LiNa_2Y(BO_3)_2$ are attributed to the asymmetric stretching of the BO_3 units, while the absorption peak at 767 cm^{-1} corresponds to the symmetric stretching of the BO_3 units. For $RbNa_2Y(BO_3)_2$, the absorption peaks at 1435 and 1190 cm^{-1} are ascribed to the asymmetric stretching of BO_3, and the symmetric stretching of trigonal BO_3 can be observed at 876 and 778 cm^{-1}. For $RbSrY(BO_3)_2$, the absorption peaks at 1179 and 773 cm^{-1} are assigned to the asymmetric stretching and symmetric stretching of BO_3 units, respectively. Moreover, the absorption peaks at 645, 644, and 617 cm^{-1} correspond to the out-of-plane bending of the BO_3 units in $LiNa_2Y(BO_3)_2$, $RbNa_2Y(BO_3)_2$ and $RbSrY(BO_3)_2$, respectively. These characteristic peaks confirm the existence of BO_3 groups in these structures.

The differential scanning calorimetry (DSC) curves are depicted in Fig. S3.† For $LiNa_2Y(BO_3)_2$ and $RbNa_2Y(BO_3)_2$, only one endothermic peak is observed at about 811 and 894 °C, respectively. For $RbSrY(BO_3)_2$, no endothermic peak was observed before 900 °C. In order to investigate the melting behavior of the three compounds, we placed the pure powder into a platinum crucible and heated it to 850 °C for $LiNa_2Y$

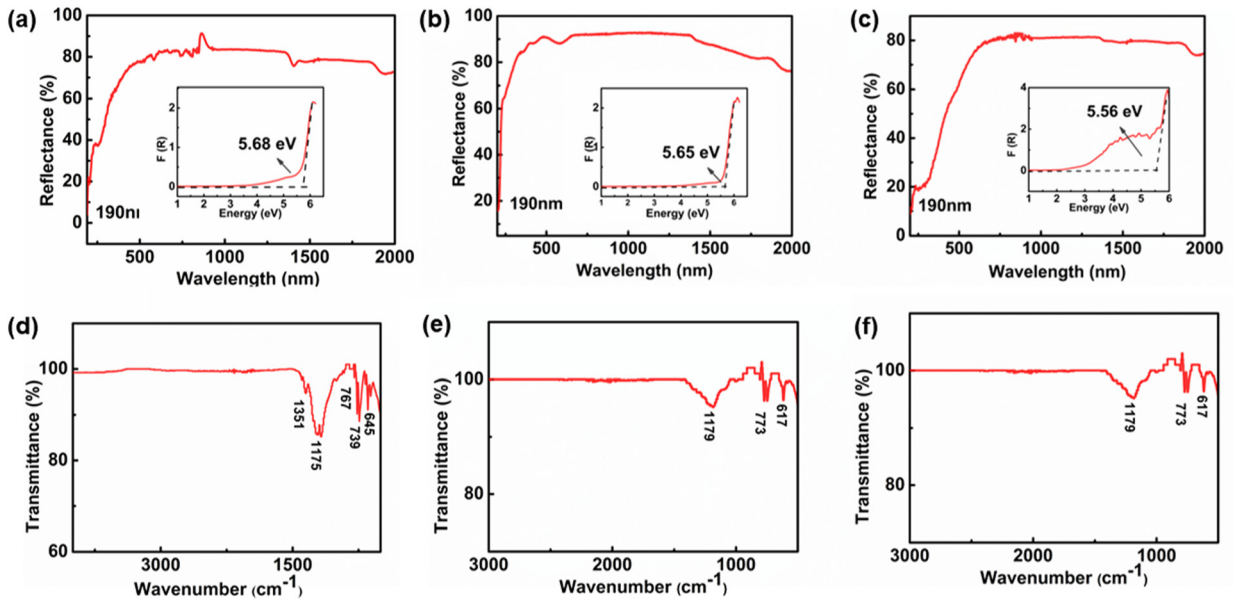

Fig. 2 UV-vis-NIR diffuse reflectance spectra of (a) $LiNa_2Y(BO_3)_2$, (b) $RbNa_2Y(BO_3)_2$, and (c) $RbSrY(BO_3)_2$. IR spectra of (d) $LiNa_2Y(BO_3)_2$, (e) $RbNa_2Y(BO_3)_2$, and (f) $RbSrY(BO_3)_2$.

$(BO_3)_2$, 950 °C for $RbNa_2Y(BO_3)_2$, and 1000 °C for $RbSrY(BO_3)_2$. Further, X-ray diffraction (XRD) analysis was conducted on calcined samples. The results indicate that $LiNa_2Y(BO_3)_2$ melts congruently while $RbNa_2Y(BO_3)_2$ and $RbSrY(BO_3)_2$ melt incongruently (Fig. S4†). The phase of $RbNa_2Y(BO_3)_2$ after melting is unknown, and the main residue is $Sr_3Y_3(BO_3)_4$ (PDF #54-1120) for $RbSrY(BO_3)_2$.

Furthermore, to elucidate the relationship between electronic structure and optical properties, first-principles calculations were carried out based on density functional theory (DFT) to determine the band gap and densities of states (DOS) of the three compounds. As illustrated in Fig. S5,† $LiNa_2Y(BO_3)_2$, $RbNa_2Y(BO_3)_2$, and $RbSrY(BO_3)_2$ are all direct band gap compounds with the calculated band gaps of 4.33, 3.25, and 4.87 eV, respectively. These values are smaller than the experimental values because the DFT method underestimates the band gap. The DOS is used to analyze the composition of the electronic structures (Fig. 3). The deep region of the valence band (VB) (−27 to −7 eV) mainly comprises Na 2p, B 2s, B 2p and O 2s orbitals for $LiNa_2Y(BO_3)_2$; Rb 2s, Na 2p, B 2s, B 2p and O 2s for $RbNa_2Y(BO_3)_2$; Rb 2s, Sr 2p, B 2s, B 2p and O 2s for $RbSrY(BO_3)_2$. As for the VB between −7 and 0 eV, the band is primarily made up of B 2s, B 2p and O 2p orbitals of all three compounds. Moreover, Na 2s, Na 2p, Rb 2s, Rb 2p, Sr 3d,

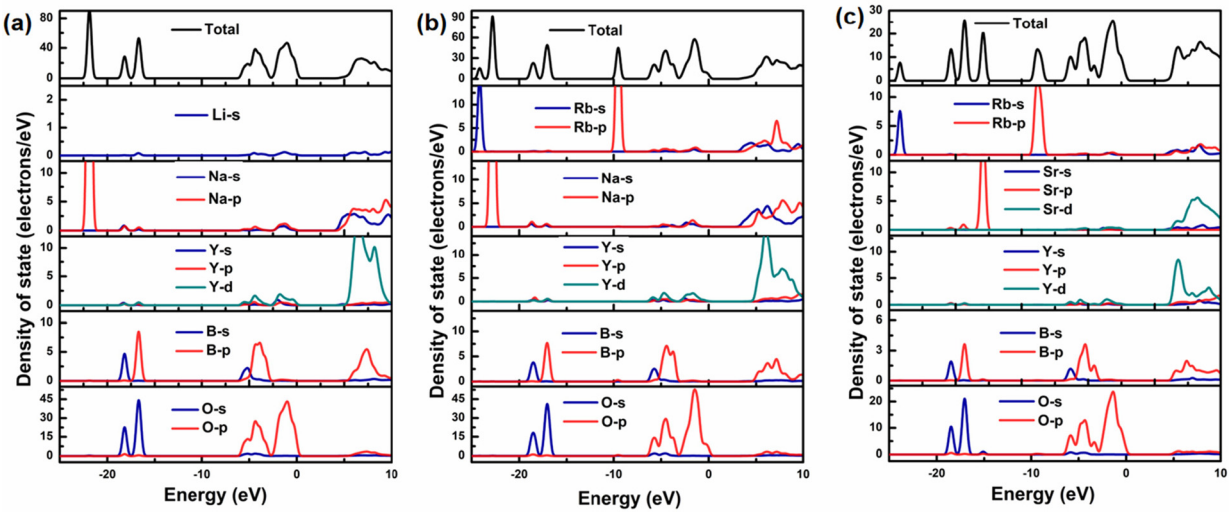

Fig. 3 Densities of states (DOS) for (a) $LiNa_2Y(BO_3)_2$, (b) $RbNa_2Y(BO_3)_2$, and (c) $RbSrY(BO_3)_2$.

Y 4d and B 2p holds a conduction band (CB) from 0 to 10 eV. In summary, the B–O groups primarily determine the optical properties near the Fermi level of the three compounds. At the same time, the birefringence was also calculated, resulting in values of 0.017, 0.033 and 0.070 at 532 nm for $LiNa_2Y(BO_3)_2$, $RbNa_2Y(BO_3)_2$, and $RbSrY(BO_3)_2$, respectively (Fig. 4).

Besides, the birefringence was measured through cross-polarization microscope based on the formula $R = \Delta n \times d$, where R, Δn, and d represent optical path difference, birefringence, and thickness, respectively. Fig. 4 shows the original interference color. The thickness measured on the Bruker single crystal diffractometer is shown in Fig. S6.† The optical path difference was obtained to be 0.45, 0.40 and 0.80 μm for $LiNa_2Y(BO_3)_2$, $RbNa_2Y(BO_3)_2$ and $RbSrY(BO_3)_2$, respectively, by comparing with the Michel–Lévy chart. Therefore, the birefringence values were determined for $LiNa_2Y(BO_3)_2$, $RbNa_2Y(BO_3)_2$, and $RbSrY(BO_3)_2$ as 0.019, 0.031 and 0.071, respectively. These experimental values are consistent with the calculated results. In addition, we have investigated Y-based borates containing isolated BO_3 in the Inorganic Crystal Structure Database (ICSD); there are 29 reported compounds (Table S4†). Only 7 compounds were reported with birefringence values, including $LiRb_2Y(BO_3)_2$, $CaRbY(BO_3)_2$, $YCa_4O(BO_3)_3$, $Na_3Y_3(BO_3)_4$, $YAl_3(BO_3)_4$, $Li_2RbY_4(BO_3)_5$ and $Li_2CsY_4(BO_3)_5$. One can find that cation substitution in isostructural structures has little effect on birefringence, such as the birefringence of 0.10@532 nm in both $Li_2RbY_4(BO_3)_5$ and $Li_2CsY_4(BO_3)_5$. On the other hand, from $LiRb_2Y(BO_3)_2$ to $CaRbY(BO_3)_2$, the cation difference results in obviously different birefringence, *i.e.*, 0.038@532 nm in $LiRb_2Y(BO_3)_2$ and $CaRbY(BO_3)_2$ (0.048@532 nm). These results demonstrate that cation substitution with significant radius differences is an important way to adjust the structural change and then regulate the birefringence. This phenomenon has also been observed in the title compounds $LiNa_2Y(BO_3)_2$, $RbNa_2Y(BO_3)_2$ and $RbSrY(BO_3)_2$.

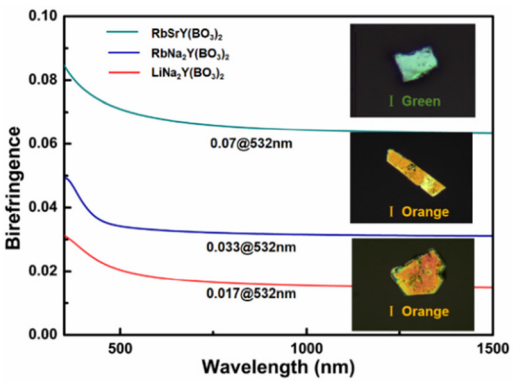

Fig. 4 Calculated and experimental birefringence for $LiNa_2Y(BO_3)_2$, $RbNa_2Y(BO_3)_2$, and $RbSrY(BO_3)_2$.

To determine the origin of birefringence in the three compounds, we will analyze from the following three aspects: the arrangement of BO_3 groups, the covalency of Y–O bonds and bonding electron density difference ($\Delta\rho$) based on the response electron distribution anisotropy (REDA) approximations.

(i) Arrangement of BO_3 groups. According to the anionic group theory, the co-planar BO_3 groups are conducive to increasing the structural anisotropy and then improving the birefringence. Based on the above structural analysis, one can find that in $LiNa_2Y(BO_3)_2$, $B(1)O_3$ and $B(2)O_3$ triangles are in the interlayers and intralayers of Y–O layers, which result in the noncoplanar arrangement of $B(1)O_3$ and $B(2)O_3$ triangles. This can be proved in Fig. 5. In $RbNa_2Y(BO_3)_2$, the $B(1)O_3$ triangles adopt a completely coplanar manner in the *ac* plane, while $B(2)O_3$ triangles are coplanar in the *bc* plane. The two planes are just perpendicular to each other, which will lead to

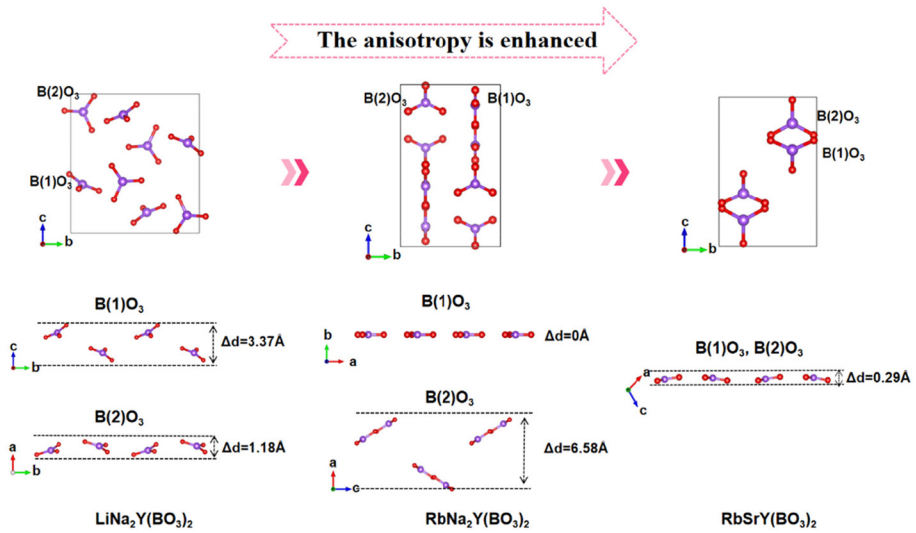

Fig. 5 Arrangement of BO_3 groups in three compounds (Δd is defined as the inclined separation distance of the BO_3 groups within a single B–O layer).

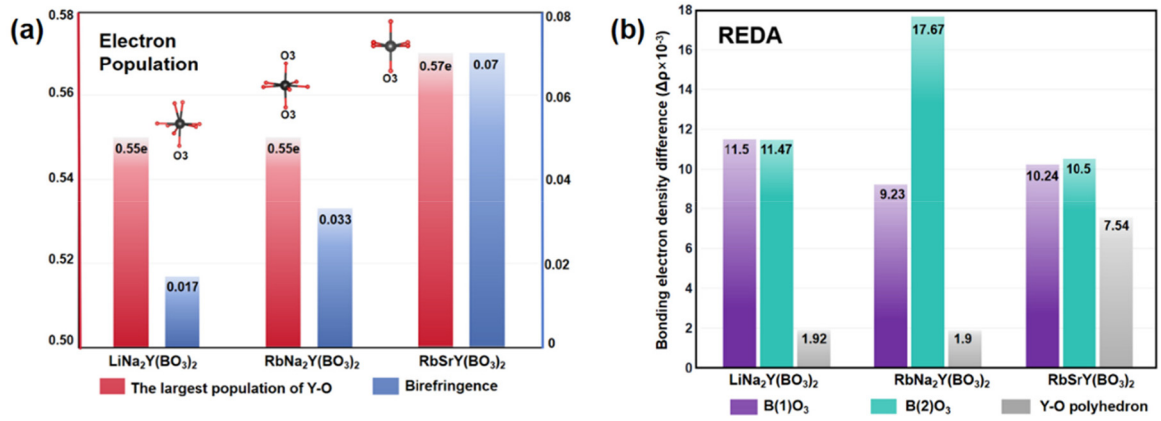

Fig. 6 (a) Calculated birefringence at 532 nm and the largest population of Y–O bonds. (b) Bonding electron density difference ($\Delta\rho$) of $LiNa_2Y(BO_3)_2$, $RbNa_2Y(BO_3)_2$, and $RbSrY(BO_3)_2$.

the overall polarization anisotropy to be partly cancelled out. In $RbSrY(BO_3)_2$, both $B(1)O_3$ and $B(2)O_3$ groups are in a coplanar configuration with an oppositely aligned arrangement. Compared to the first two structures, the high density and the coplanar arrangement of BO_3 groups facilitate the superposition for polarization anisotropy in $RbSrY(BO_3)_2$.

(ii) Electronic population of Y–O polyhedra. The overlap populations represent the density distribution of electrons in different atomic orbitals, and in general, the larger the population value, the more overlapping charges between two atoms, that is, the greater the degree of covalent bond formation. If the bond has a population value larger than 0.5*e* (charge unit), it indicates that the bond is more covalent. In $LiNa_2Y(BO_3)_2$, $RbNa_2Y(BO_3)_2$ and $RbSrY(BO_3)_2$, electronic population results show that Y–O bonds have a large population, with the maximum values of 0.55, 0.55 and 0.57*e* for $LiNa_2Y(BO_3)_2$, $RbNa_2Y(BO_3)_2$ and $RbSrY(BO_3)_2$, respectively (Table S5†). Especially in $RbSrY(BO_3)_2$, the Y(1)–O(1), Y(1)–O(3) and Y(1)–O(4) all exhibit large population, indicating that there is covalent interaction between Y and O in YO_6 polyhedra, which will have a significant effect on the optical properties.

(iii) Bonding electron density difference ($\Delta\rho$) calculation. To characterize optical anisotropy, the $\Delta\rho$ of Y–O polyhedra and BO_3 was calculated. The results show that the $\Delta\rho$ values of $B(1)O_3$, $B(2)O_3$ were 11.5, 11.47 $\times$ 10^{-3} for $LiNa_2Y(BO_3)_2$, 9.23, 17.67 $\times$ 10^{-3} for $RbNa_2Y(BO_3)_2$ and 10.24, 10.5 $\times$ 10^{-3} for $RbSrY(BO_3)_2$, respectively. The values of Y–O polyhedra were 1.92, 1.9, 7.54 $\times$ 10^{-3} for $LiNa_2Y(BO_3)_2$, $RbNa_2Y(BO_3)_2$ and $RbSrY(BO_3)_2$, respectively (Fig. 6b). These indicate that BO_3 is the main source of birefringence properties in these three compounds. Meanwhile, the contributions of Y–O polyhedra cannot be ignored, especially in $RbSrY(BO_3)_2$, where the YO_6 octahedron with strong covalent bonds contributes almost 26.7% to anisotropy. Thus, we infer that the different arrangement of BO_3 anion groups and the Y–O polyhedra with strong covalent bonds caused by the cation substitution play an important role in the significant difference in birefringence among $LiNa_2Y(BO_3)_2$, $RbNa_2Y(BO_3)_2$ and $RbSrY(BO_3)_2$.

Conclusions

In summary, we have successfully synthesized three Y-based borates with isolated BO_3, $LiNa_2Y(BO_3)_2$, $RbNa_2Y(BO_3)_2$, and $RbSrY(BO_3)_2$. All these compounds exhibit a short UV cutoff edge (<190 nm), which holds great promise for applications in DUV optical materials. The DSC and powder XRD measurement indicate that $LiNa_2Y(BO_3)_2$ is a congruent melting compound, which favors the growth of a large crystal. IR spectra confirm the existence of BO_3 in their structures. With the substitution of cations, the birefringence shows an increasing trend from $LiNa_2Y(BO_3)_2$ and $RbNa_2Y(BO_3)_2$ to $RbSrY(BO_3)_2$. In particular, $RbSrY(BO_3)_2$ exhibits a large birefringence, ~4 times that of $LiNa_2Y(BO_3)_2$, which is rarely reported in rare-earth borates. Structural analyses and theoretical calculations indicate that the birefringence difference among these three compounds can be ascribed to the different arrangement of BO_3 anion groups and the Y–O polyhedra with strong covalent bonds, which is caused by the cation substitution. The results demonstrate the potential regulatory effect of cations on birefringence, that is, the substitution of large size and high coordination cations assembles the arrangement of functional units and further improves the structural anisotropy, thereby increasing the birefringence. This work presents an effective route for designing novel UV/DUV materials with enhanced birefringence.

Author contributions

Writing – original draft: Guanglian Sun; Writing – review & editing: Hongping Wu; Resources: Zhanggui Hu; Supervision: Jiyang Wang and Yicheng Wu.

Conflicts of interest

There are no conflicts to declare.

Acknowledgements

This work is supported by the National Natural Science Foundation of China (Grant No. 52322202 and 22071179), Natural Science Foundation of Tianjin (Grant No. 20JCJQJC00060 and 21JCJQJC00090).

References

1 P. F. Li, C. L. Hu, F. Kong and J. G. Mao, The First UV Nonlinear Optical Selenite Material: Fluorination Control in $CaYF(SeO_3)_2$ and $Y_3F(SeO_3)_4$, *Angew. Chem., Int. Ed.*, 2023, **62**, e202301420.

2 G. A. Ermolaev, D. V. Grudinin, Y. V. Stebunov, K. V. Voronin, V. G. Kravets, J. Duan, A. B. Mazitov, G. I. Tselikov, A. Bylinkin, D. I. Yakubovsky, S. M. Novikov, D. G. Baranov, A. Y. Nikitin, I. A. Kruglov, T. Shegai, P. Alonso-González, A. N. Grigorenko, A. V. Arsenin, K. S. Novoselov and V. S. Volkov, Giant optical anisotropy in transition metal dichalcogenides for next-generation photonics, *Nat. Commun.*, 2021, **12**, 854.

3 X. L. Chen, B. B. Zhang, F. F. Zhang, Y. Wang, M. Zhang, Z. H. Yang, K. R. Poeppelmeier and S. L. Pan, Designing an Excellent Deep-Ultraviolet Birefringent Material for Light Polarization, *J. Am. Chem. Soc.*, 2018, **140**, 16311–16319.

4 S. Liu, X. M. Liu, S. G. Zhao, Y. C. Liu, L. N. Li, Q. R. Ding, Y. Q. Li, Z. S. Lin, J. H. Luo and M. C. Hong, An Exceptional Peroxide Birefringent Material Resulting from d-π Interactions, *Angew. Chem., Int. Ed.*, 2020, **59**, 9414–9417.

5 F. H. Ding, K. J. Griffith, W. G. Zhang, S. X. Cui, C. Zhang, Y. R. Wang, K. Kamp, H. W. Yu, P. S. Halasyamani, Z. H. Yang, S. L. Pan and K. R. Poeppelmeier, $NaRb_6(B_4O_5(OH)_4)_3(BO_2)$ Featuring Noncentrosymmetry, Chirality, and the Linear Anionic Group BO_2^-, *J. Am. Chem. Soc.*, 2023, **145**, 4928–4933.

6 X. H. Dong, L. Huang, H. M. Zeng, Z. E. Lin, K. M. Ok and G. H. Zou, High-Performance Sulfate Optical Materials Exhibiting Giant Second Harmonic Generation and Large Birefringence, *Angew. Chem., Int. Ed.*, 2022, **61**, e202116790.

7 J. Lu, Y. K. Lian, L. Xiong, Q. R. Wu, M. Zhao, K. X. Shi, L. Chen and L. M. Wu, How To Maximize Birefringence and Nonlinearity of π-Conjugated Cyanurates, *J. Am. Chem. Soc.*, 2019, **141**, 16151–16159.

8 B. L. Wu, C. L. Hu, F. F. Mao, R. L. Tang and J. G. Mao, Highly Polarizable Hg^{2+} Induced a Strong Second Harmonic Generation Signal and Large Birefringence in $LiHgPO_4$, *J. Am. Chem. Soc.*, 2019, **141**, 10188–10192.

9 G. Q. Shi, Y. Wang, F. F. Zhan, B. B. Zhang, R. H. Yang, X. L. Hou, S. L. Pan and K. R. Poeppelmeier, Finding the Next Deep-Ultraviolet Nonlinear Optical Material: $NH_4B_4O_6F$, *J. Am. Chem. Soc.*, 2017, **139**, 10645–10648.

10 Y. Wang, B. B. Zhang, Z. H. Yang and S. L. Pan, Cation-Tuned Synthesis of Fluorooxoborates: Towards Optimal Deep-Ultraviolet Nonlinear Optical Material, *Angew. Chem., Int. Ed.*, 2018, **57**, 2150–2154.

11 X. X. Jiang, S. Y. Luo, L. Kang, P. F. Gong, H. W. Huang, S. C. Wang, Z. S. Lin and C. T. Chen, First-Principles Evaluation of the Alkali and/or Alkaline Earth Beryllium Borates in Deep Ultraviolet Nonlinear Optical Applications, *ACS Photonics*, 2015, **2**, 1183–1191.

12 X. F. Wang, X. D. Leng, Y. Kuk, J. Lee, Q. Jing and K. M. Ok, Deep-Ultraviolet Transparent Mixed Sulfamates with Enhanced Nonlinear Optical Properties and Birefringence, *Angew. Chem., Int. Ed.*, 2024, **63**, e202315434.

13 X. H. Meng, F. Liang, K. J. Kang, J. Tang, Q. Huang, W. L. Yin, Z. S. Lin and M. J. Xia, A rich structural chemistry in π-conjugated hydroisocyanurates: layered structures of $A_2B(H_2C_3N_3O_3)_4{\cdot}nH_2O$ (A = K, Rb, Cs; B = Mg, Ca; n = 4, 10) with high ultraviolet transparency and strong optical anisotropy, *Dalton Trans.*, 2019, **48**, 9048–9052.

14 H. P. Wu, H. W. Yu, Z. H. Yang, X. L. Hou, X. Su, S. L. Pan, K. R. Poeppelmeier and J. M. Rondinelli, Designing a Deep Ultraviolet Nonlinear Material with a Large Second Harmonic Generation Response, *J. Am. Chem. Soc.*, 2013, **135**, 4215–4218.

15 H. T. Luo, T. Tkaczyk, E. L. Dereniak, K. Oka and R. Sampson, High birefringence of the yttrium vanadate crystal in the middle wavelength infrared, *Opt. Lett.*, 2006, **31**, 616–618.

16 J. R. DeVore, Refractive Indices of Rutile and Sphalerite, *J. Opt. Soc. Am.*, 1951, **41**, 416–419.

17 R. V. Schmidt and I. P. Kaminow, Metal-diffused optical Waveguides in $LiNbO_3$, *Appl. Phys. Lett.*, 1974, **25**, 458–460.

18 G. Ghosh, Dispersion-equation coefficients for the refractive index and birefringence of calcite and quartz crystals, *Opt. Commun.*, 1999, **163**, 95–102.

19 H. N. Liu, H. P. Wu, Z. G. Hu, J. Y. Wang, Y. C. Wu and H. W. Yu, $Cs_3[(BOP_2)(B_3O_7)_3]$: A Deep-Ultraviolet Nonlinear Optical Crystal Designed by Optimizing Matching of Cation and Anion Groups, *J. Am. Chem. Soc.*, 2023, **145**, 12691–12700.

20 Y. Y. Yang, Y. Guo, Y. G. Chen, X. W. Hu, X. Zhang and X. M. Zhang, Hexameric poly-fluoroberyllophosphate $Na_4Be_2PO_4F_5$ with moderate birefringence and deep-ultraviolet transmission as a potential zero-order-waveplate crystal, *Inorg. Chem. Front.*, 2022, **9**, 5469–5477.

21 J. J. Zhou, H. P. Wu, H. W. Yu, S. T. Jiang, Z. G. Hu, J. Y. Wang, Y. C. Wu and P. S. Halasyamani, $BaF_2TeF_2(OH)_2$, *J. Am. Chem. Soc.*, 2020, **142**, 4616–4620.

22 C. Wu, X. X. Jiang, Z. J. Wang, L. Lin, Z. S. Lin, Z. P. Huang, X. F. Long, M. G. Humphrey and C. Zhang, Giant Optical Anisotropy in the UV-Transparent 2D Nonlinear Optical Material $Sc(IO_3)_2(NO_3)$, *Angew. Chem., Int. Ed.*, 2021, **60**, 3464–3468.

23 M. J. Dodge, Refractive properties of magnesium fluoride, *Appl. Opt.*, 1984, **23**, 1980–1985.

24 X. F. Wang, Y. Wang, B. B. Zhang, F. F. Zhang, Z. H. Yang and S. L. Pan, CsB_4O_6F: A Congruent-Melting Deep-Ultraviolet Nonlinear Optical Material by Combining

Superior Functional Units, *Angew. Chem., Int. Ed.*, 2017, **56**, 14119–14123.

25 Y. Long, X. H. Dong, L. Huang, H. M. Zeng, Z. Lin and G. H. Zou, $SbHPO_3F$: 2D van der Waals Layered Phosphite Exhibiting Large Birefringence, *Inorg. Chem.*, 2022, **61**, 16997–17001.

26 J. K. Wang, Y. S. Cheng, H. P. Wu, Z. G. Hu, J. Y. Wang, Y. C. Wu and H. W. Yu, $Sr_3[SnOSe_3]$ $[CO_3]$: A Heteroanionic Nonlinear Optical Material Containing Planar π-conjugated $[CO_3]$ and Heteroleptic $[SnOSe_3]$ Anionic Groups, *Angew. Chem., Int. Ed.*, 2022, **61**, e202201616.

27 X. H. Meng, F. Liang, J. Tang, K. J. Kang, W. L. Yin, T. X. Zeng, B. Kang, Z. S. Lin and M. J. Xia, LiO_4 tetrahedra lock the alignment of π-conjugated layers to maximize optical anisotropy in metal hydroisocyanurates, *Inorg. Chem. Front.*, 2019, **6**, 2850–2854.

28 Y. J. Zhang, Q. Bian, H. P. Wu, H. W. Yu, Z. G. Hu, J. Y. Wang and Y. C. Wu, Designing A New Infrared Nonlinear Optical Material, β-$BaGa_2Se_4$ Inspired by the Phase Transition of the BaB_2O_4(BBO), *Angew. Chem., Int. Ed.*, 2022, **61**, e202115374.

29 J. H. Kim, J. Baek and P. S. Halasyamani, $(NH_4)_2Te_2WO_8$: A new polar oxide with second-harmonic generating, ferroelectric, and pyroelectric properties, *Chem. Mater.*, 2007, **19**, 5637–5641.

30 Y. Yang, Y. Qiu, P. F. Gong, L. Kang, G. M. Song, X. M. Liu, J. L. Sun and Z. S. Lin, Lone-Pair Enhanced Birefringence in an Alkaline-Earth MetalTin(II) Phosphate $BaSn_2(PO_4)_2$, *Chem. – Eur. J.*, 2019, **25**, 5648–5651.

31 Y. Chu, H. S. Wang, T. Abutukadi, Z. Li, M. Mutailipu, X. Su, Z. H. Yang, J. J. Li and S. L. Pan, $Zn_2HgP_2S_8$: A Wide Bandgap Hg-Based Infrared Nonlinear Optical Material with Large Second-Harmonic Generation Response, *Small*, 2023, **19**, 2305074.

32 C. B. Jiang, X. X. Jiang, C. Wu, Z. P. Huang, Z. S. Lin, M. G. Humphrey and C. Zhang, Isoreticular Design of $KTiOPO_4$-Like Deep-Ultraviolet Transparent Materials Exhibiting Strong Second-Harmonic Generation, *J. Am. Chem. Soc.*, 2022, **144**, 20394–20399.

33 Y. Chu, H. S. Wang, Q. Chen, X. Su, Z. X. Chen, Z. H. Yang, J. J. Li and S. L. Pan, "Three-in-One": A New Hg-Based Selenide $Hg_7P_2Se_{12}$ Exhibiting Wide Infrared Transparency Range and Strong Nonlinear Optical Effect, *Adv. Funct. Mater.*, 2023, **34**, 202314933.

34 J. J. Zhang, Z. H. Zhang, Y. X. Sun, C. Q. Zhang and X. T. Tao, Bulk crystal growth and characterization of a new polar polymorph of $BaTeMo_2O_9$: α-$BaTeMo_2O_9$, *CrystEngComm*, 2011, **13**, 6985–6990.

35 K. C. Chen, C. S. Lin, J. D. Chen, G. S. Yang, H. T. Tian, M. Luo, T. Yan, Z. G. Hu, J. Y. Wang, Y. C. Wu, N. Ye and G. Peng, Intense *d-p* Hybridization in Nb_3O_{15} Tripolymer Induced the Largest Second Harmonic Generation Response and Birefringence in Germanates, *Angew. Chem., Int. Ed.*, 2023, **62**, e202217039.

36 J. Y. Guo, A. Tudi, S. J. Han, Z. H. Yang and S. L. Pan, $Sn_2B_5O_9Cl$: A Material with Large Birefringence Enhancement Activated Prepared via Alkaline-Earth-Metal Substitution by Tin, *Angew. Chem., Int. Ed.*, 2019, **58**, 17675–17678.

37 P. F. Li, C. L. Hu, Y. F. Li, J. G. Mao and F. Kong, $Hg_4(Te_2O_5)$ (SO_4): A Giant Birefringent Sulfate Crystal Triggered by a Highly Selective Cation, *J. Am. Chem. Soc.*, 2024, **146**, 7868–7874.

38 C. Wu, X. X. Jiang, L. Lin, Y. L. Hu, T. H. Wu, Z. S. Lin, Z. P. Huang, M. G. Humphrey and C. Zhang, A Congruent-Melting Mid-Infrared Nonlinear Optical Vanadate Exhibiting Strong Second-Harmonic Generation, *Angew. Chem., Int. Ed.*, 2021, **60**, 22447–22453.

39 H. P. Wu, H. W. Yu, S. L. Pan, Z. J. Huang, Z. H. Yang, X. Su and K. R. Poeppelmeier, $Cs_2B_4SiO_9$: A Deep-Ultraviolet Nonlinear Optical Crystal, *Angew. Chem., Int. Ed.*, 2013, **52**, 3406–3410.

40 C. Wu, C. B. Jiang, G. F. Wei, X. X. Jiang, Z. J. Wang, Z. S. Lin, Z. P. Huang, M. G. Humphrey and C. Zhang, Toward Large Second-Harmonic Generation and Deep-UV Transparency in Strongly Electropositive Transition Metal Sulfates, *J. Am. Chem. Soc.*, 2023, **145**, 3040–3046.

41 X. Wang, M. J. Xia and P. K. Li, A promising birefringent crystal $Ba_2Na_3(B_3O_6)_2F$, *Opt. Mater.*, 2014, **38**, 6–9.

42 S. C. Wang and N. Ye, $Na_2CsBe_6B_5O_{15}$: An Alkaline Beryllium Borate as a Deep-UV Nonlinear Optical Crystal, *J. Am. Chem. Soc.*, 2011, **133**, 11458–11461.

43 S. G. Zhao, P. F. Gong, L. Bai, X. Xu, S. Q. Zhang, Z. H. Sun, Z. S. Lin, M. C. Hong, C. T. Chen and J. H. Luo, Beryllium-free $Li_4Sr(BO_3)_2$ for deep-ultraviolet nonlinear optical application, *Nat. Commun.*, 2014, **5**, 5019.

44 J. J. Zhou, Y. Q. Liu, H. P. Wu, H. W. Yu, Z. S. Lin, Z. G. Hu, J. Y. Wang and Y. C. Wu, $CsZn_2BO_3X_2$(X_2=F_2, Cl_2, and FCl): A Series of Beryllium-Free Deep-Ultraviolet Nonlinear-Optical Crystals with Excellent Properties, *Angew. Chem., Int. Ed.*, 2020, **59**, 19006–19010.

45 M. G. Gao, Q. Bian, H. P. Wu, H. W. Yu, Z. G. Hu, J. Y. Wang and Y. C. Wu, Inducing large birefringence by enhancing asymmetric electron distribution of Y-O polyhedra, *Inorg. Chem. Front.*, 2022, **9**, 1956–1963.

46 J. F. Zhou, P. F. Gong, M. J. Xia, A. M. Ji, L. F. Zhang, H. Q. Wu and Q. Wu, Atomic Substitution to Tune ScO_6 Distortion in $Ba_2MSc_2(BO_3)_4$ (M = Na, K, Ba) to Acquire a Large Birefringence, *Inorg. Chem.*, 2023, **62**, 8931–8939.

47 M. O'Keeffe and N. E. Brese, Bond-valence parameters for anion-anion bonds in solids, *Acta Crystallogr., Sect. B: Struct. Sci.*, 1992, **48**, 152–154.

48 R. D. Shanno, Revised Effective Ionic Radii and Systematic Studies of Interatomic Distances in Halides and Chalcogendies, *Acta Crystallogr., Sect. A: Found. Adv.*, 1976, **32**, 751.

49 S. G. Zhao, G. C. Zhang, J. Y. Yao and Y. C. Wu, $K_3YB_6O_{12}$: A new nonlinear optical crystal with a short UV cutoff edge, *Mater. Res. Bull.*, 2012, **47**, 3810–3813.

50 H. J. Zhang, X. L. Meng, L. Zhu, C. Q. Wang, R. P. Cheng, W. T. Yu, S. J. Zhang, L. K. Sun, Y. T. Chow, W. L. Zhang, H. Wang and K. S. Wong, Growth and laser properties of Nd:$Ca_4YO(BO_3)_3$ crystal, *Opt. Commun.*, 1999, **160**, 273–276.

51 M. Mutailipu, Z. Q. Xie, X. Su, M. Zhang, Y. Wang and Z. H. Yang, MRSA. Janjua, and S. L. Pan, Chemical Cosubstitution-Oriented Design of Rare-Earth Borates as Potential Ultraviolet Nonlinear Optical Materials, *J. Am. Chem. Soc.*, 2017, **139**, 18397–18405.